## RESEARCH ARTICLE

Check for updates

# Water-compatible fluorescent [2]rotaxanes for Au³⁺ detection and bioimaging†

Sing-Ming Chan,[a] Fung-Kit Tang,[a] Chak-Shing Kwan,[a] Ching-Yau Lam,[a] Sam C. K. Hau[b] and Ken Cham-Fai Leung (ID) *[a]

In this study, the synthesis of [2]rotaxanes as fluorescent metal ion sensors has been demonstrated. [2]Rotaxanes, **RA**-H·PF₆, **RRA** and **RRB**, undergo photoelectron transfer resulting in fluorescence quenching. Before the diimine (dynamic covalent bond) reduction on the macrocyclic ring, the dynamic [2]rotaxane **RA**-H·PF₆ can be hydrolyzed and turned fluorescent by trivalent metal ions, giving fluorescence at $\lambda_{max}$ 424 nm. After reduction of the imines, the reduced [2]rotaxanes **RRA** and **RRB** are kinetically stable and highly selective to Au³⁺ binding among 27 metal ions in a water-compatible (50 vol%) solution with working fluorescence in the range of pH 4–10. 50-Fold and 1.2-fold fluorescence turn-on after addition of Au³⁺ has been observed for **RRA** and **RRB**, respectively. Metal interference on Au³⁺ detection is insignificant, and thereby the fluorescence intensity is linearly proportional to the concentration of Au³⁺ until excess. The solid-state crystal structure of **RRA** shows the mechanically interlocked structure (mechanical bond). The bioimaging experiment of **RRB** with HeLa cells demonstrates the potential application of these mechanically interlocked molecules for metal ion detection in aqueous media and biological systems.

## Introduction

Simple organic molecules have been used as fluorescent metal ion sensors due to their high selectivity, sensitivity, simplicity, quick response and feasibility of both *in vitro* and *in vivo* testing.[1–4] In particular, rotaxanes, mechanically interlocked molecules with unique topology,[5,6] have been in the spotlight for ion sensing over the past few decades. Compared to conventional sensors, the interlocked system of rotaxanes can provide a dynamic and yet switchable cavity, thus allowing them to bind specific analytes selectively.[7] The mechanical bond can also provide unusual coordination geometries and augmented redox activity as a potential ligand.[8] It was first reported by Hiratani and co-workers as a selective Li⁺ fluorescent rotaxane sensor in CH₂Cl₂/MeCN solution (90 : 10, v/v).[9] Previously, Goldup and co-workers reported a [2]rotaxane fluorescent sensor for Zn²⁺ in MeCN/H₂O solution (98 : 2, v/v).[10] In another study performed by Beer and co-workers, they designed a rotaxane for sensing halide ions in up to 35% H₂O in MeCN.[11] Lin and co-workers also reported a [2]rotaxane for Fe³⁺ detection

and bioimaging.[12] However, most of the rotaxane sensors focus on alkali metal ions,[9,13,14] divalent transition metal ions[10,15] and anions.[11,16–18] In the case of precious metals and other platinum group elements (Pt, Pd, Rh, Ir, Ru, and Os), the application of using rotaxanes as a metal ion sensor in aqueous media is relatively unexplored, and thereby the effect of other metal ions as interference is seldom mentioned.[10] Since the detection of metal ions in aqueous media has become crucial in biological systems, the development of water-soluble rotaxane metal ion sensors has become highly desired.

Gold, one of the precious metals, has been utilized in functional nanoparticles.[19] In particular, its ion form, Au³⁺, has been applied in biological,[20,21] catalysis,[22,23] and other industrial applications.[24] For instance, recent studies have shown that an Au(III) complex could be used as an effective anticancer drug due to its tumor growth inhibiting properties.[21] Despite the advantages, excess Au³⁺ can damage the organs.[25] For example, Au³⁺ can lead to inhibition of the oxygen consumption of liver and kidney slices.[26] An Au³⁺ salt solution is over 90% toxic at a concentration of 200 μM.[27] Thus, the detection of Au³⁺ has become crucial.

Herein, we report fluorescent [2]rotaxanes as selective metal ion sensors for detecting Au³⁺ and other trivalent metal ions in aqueous media by applying dynamic clipping on R₂NH₂⁺ for [2]rotaxane synthesis. It is part of dynamic covalent chemistry (DCC), which allows self-error checking and self-sorting to give the most thermodynamically stable rotaxane as the major product.[28–36]

[a] *Department of Chemistry, Hong Kong Baptist University, Kowloon Tong, Kowloon, Hong Kong SAR, P. R. China. E-mail: cfleung@hkbu.edu.hk*

[b] *Department of Chemistry, The Chinese University of Hong Kong, Shatin, New Territories, Hong Kong SAR, P. R. China*

The rotaxanes reported in this project were obtained in high yield, having pyridine/amine nitrogen and ethylene glycol oxygen donor atom moieties for selective metal ion binding. First, the fluorescent response of the as-synthesized **RA**-H·PF$_6$ and **RB**-H·PF$_6$ with the trivalent metal ions in 1% H$_2$O in MeCN was investigated. To increase the selectivity, **RA**-H·PF$_6$ and **RB**-H·PF$_6$ were further reduced, and the fluorescence response shows much significant improvement for **RRA** and **RRB** on detection of Au$^{3+}$ ions in MeCN/H$_2$O solution. In view of potential bio-application of rotaxanes such as drug delivery,[37–40] the cell viability of HeLa cells was performed to demonstrate the *in vitro* imaging of Au$^{3+}$ with both **RRA** and **RRB**.

## Results and discussion

As shown in Scheme 1, two dynamic rotaxanes, **RA**-H·PF$_6$ and **RB**-H·PF$_6$, were first synthesized for trivalent metal ion sensing. **RA**-H·PF$_6$ was thermodynamically formed *via* a clipping strategy with equal molar concentrations of tetraethylene glycol bis(2-aminophenyl)ether (diamine **1**), 2,6-pyridine dicarboxaldehyde (dialdehyde **2**) and anthracene-based axle **3**.[41] On the other hand, **RB**-H·PF$_6$ was synthesized with **1**, **2**, and BODIPY-based axle **4** by using the same clipping strategy. After the [2]rotaxane formation, the original fluorescence from the anthracene-based and BODIPY-based axles could be quenched, which may be caused by the electron transfer from the imine and pyridine moieties within the macrocyclic ring. The fluorescence could be restored when the imine moieties of **RA**-H·PF$_6$ hydrolyze back to the aldehyde and amine groups in the presence of acid or water, which leads to the dissociation of the macrocycle and separate components. The breakdown will then inhibit the internal electron transfer and provide a fluorescence band with $\lambda_{max}$ at 424 nm.

The fluorescence response of **RA**-H·PF$_6$ towards cations Li$^+$, NH$_4^+$, Na$^+$, K$^+$, Ag$^+$, Cs$^+$, Mg$^{2+}$, Ca$^{2+}$, Mn$^{2+}$, Fe$^{2+}$, Co$^{2+}$, Ni$^{2+}$, Cu$^{2+}$, Zn$^{2+}$, Pd$^{2+}$, Cd$^{2+}$, Pt$^{2+}$, Hg$^{2+}$, Pb$^{2+}$, Al$^{3+}$, V$^{3+}$, Cr$^{3+}$, Fe$^{3+}$, Ru$^{3+}$, Rh$^{3+}$, Ce$^{3+}$, Ir$^{3+}$ and Au$^{3+}$ was first investigated in a MeCN/H$_2$O (99:1, v/v) co-solvent system. As shown in Fig. 1, the fluorescence of **RA**-H·PF$_6$ was turned on significantly by 5 equivalents
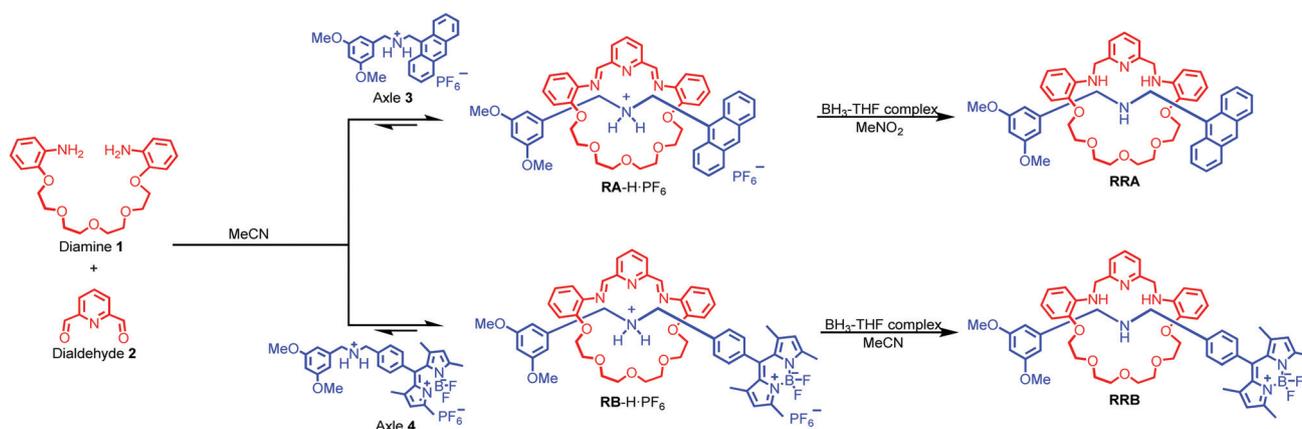


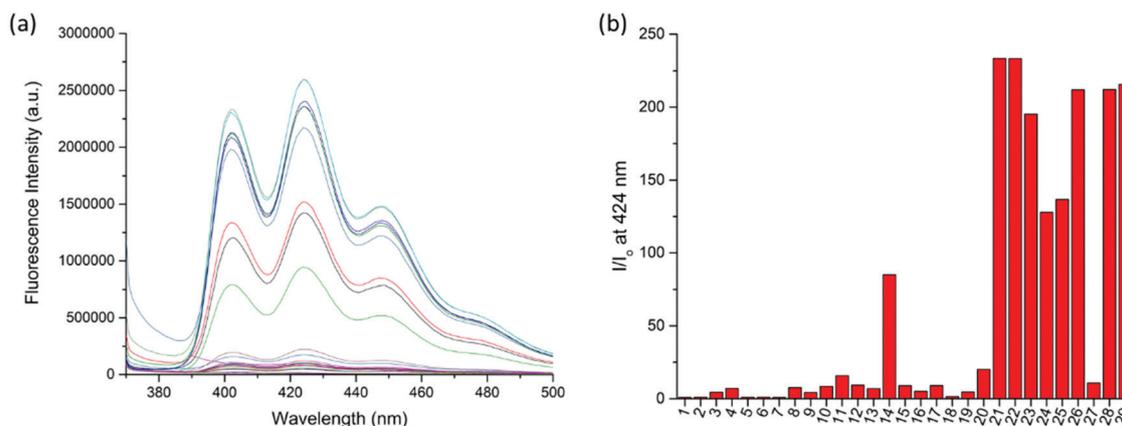**Scheme 1** Synthesis of [2]rotaxanes with anthracene and BODIPY as a stopper and fluorophore.



**Fig. 1** (a) Fluorescence spectra of **RA**-H·PF$_6$ (20 μM, $\lambda_{ex}$ = 360 nm) upon addition of 5 equiv. of M$^{n+}$ in MeCN/H$_2$O solution (99:1, v/v). (b) Fluorescence response of **RA**-H·PF$_6$ (20 μM, $\lambda_{ex}$ = 360 nm) to 5 equiv. of M$^{n+}$ at 424 nm. (1) Blank, (2) Li$^+$, (3) NH$_4^+$, (4) Na$^+$, (5) K$^+$, (6) Ag$^+$, (7) Cs$^+$, (8) Mg$^{2+}$, (9) Ca$^{2+}$, (10) Mn$^{2+}$, (11) Fe$^{2+}$, (12) Co$^{2+}$, (13) Ni$^{2+}$, (14) Cu$^{2+}$, (15) Zn$^{2+}$, (16) Pd$^{2+}$, (17) Cd$^{2+}$, (18) Pt$^{2+}$, (19) Hg$^{2+}$, (20) Pb$^{2+}$, (21) Al$^{3+}$, (22) V$^{3+}$, (23) Cr$^{3+}$, (24) Fe$^{3+}$, (25) Ru$^{3+}$, (26) Rh$^{3+}$, (27) Ce$^{3+}$, (28) Ir$^{3+}$ and (29) Au$^{3+}$.
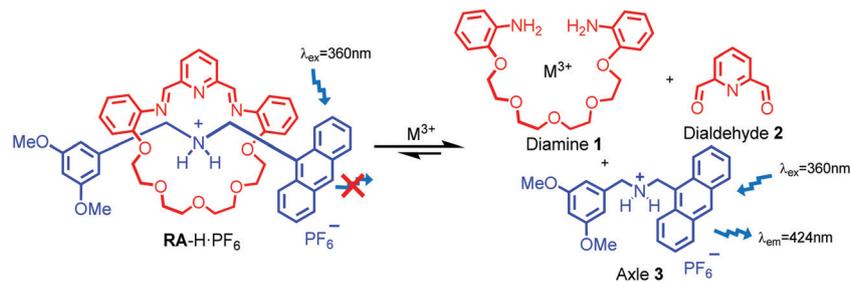
**Scheme 2** Plausible mechanism of switch on fluorescence of **RA**-H·PF$_6$ to trivalent metal ions *via* rotaxane dissociation.

of common trivalent metal ions like Al$^{3+}$, V$^{3+}$, Cr$^{3+}$, Fe$^{3+}$, Ru$^{3+}$, Rh$^{3+}$, Ir$^{3+}$ and Au$^{3+}$, along with moderate fluorescence turn-on by a divalent metal ion (Cu$^{2+}$). These results indicate that dynamic [2]rotaxane **RA**-H·PF$_6$ is relatively selective to reported trivalent metal ion binding. Al, V, Cr, and Fe are high abundance elements on Earth. Ru, Rh, Ir and Au are commonly used as catalysts for organic reactions. Since those trivalent metal ions are Lewis acids, they could induce acid hydrolysis of the imine moiety of **RA**-H·PF$_6$ upon binding to the dynamic [2]rotaxane (Scheme 2). To study the mechanism, NMR spectroscopic titration experiments were conducted. The stacked $^1$H NMR spectra (Fig. 2) illustrate that the addition of trivalent metal ions could decrease the amount of imine protons of **RA**-H·PF$_6$ while increasing the amount of aldehyde protons. This also supports that the hydrolyzed **RA**-H·PF$_6$ could be separated into diamine, dialdehyde and axle components upon the

addition of trivalent metal ions. Moreover, the axle **3** could restore its fluorescence because of the absence of PET.

With the aim to investigate another metal sensing mechanism without cleavage of the macrocyclic ring of dynamic [2]rotaxane, the imine moieties on the macrocycle of the dynamic [2]rotaxane **RA**-H·PF$_6$ and **RB**-H·PF$_6$ were then reduced by BH$_3$–THF complex (Scheme 1), yielding diamine-based, kinetically stable [2]rotaxanes **RRA** and **RRB**. After the purification by column chromatography, **RRA** and **RRB** were obtained in 70% and 75% yield, respectively. The X-ray crystallography analysis of **RRA** single crystal shows the existence of the interlocking structure (mechanical bond) in the solid-state structure (Fig. 3), confirming successful diimine reduction to form the **RRA**.

The selectivity of the reduced rotaxanes to cations was investigated. Since the solubility of **RRA** is relatively low at
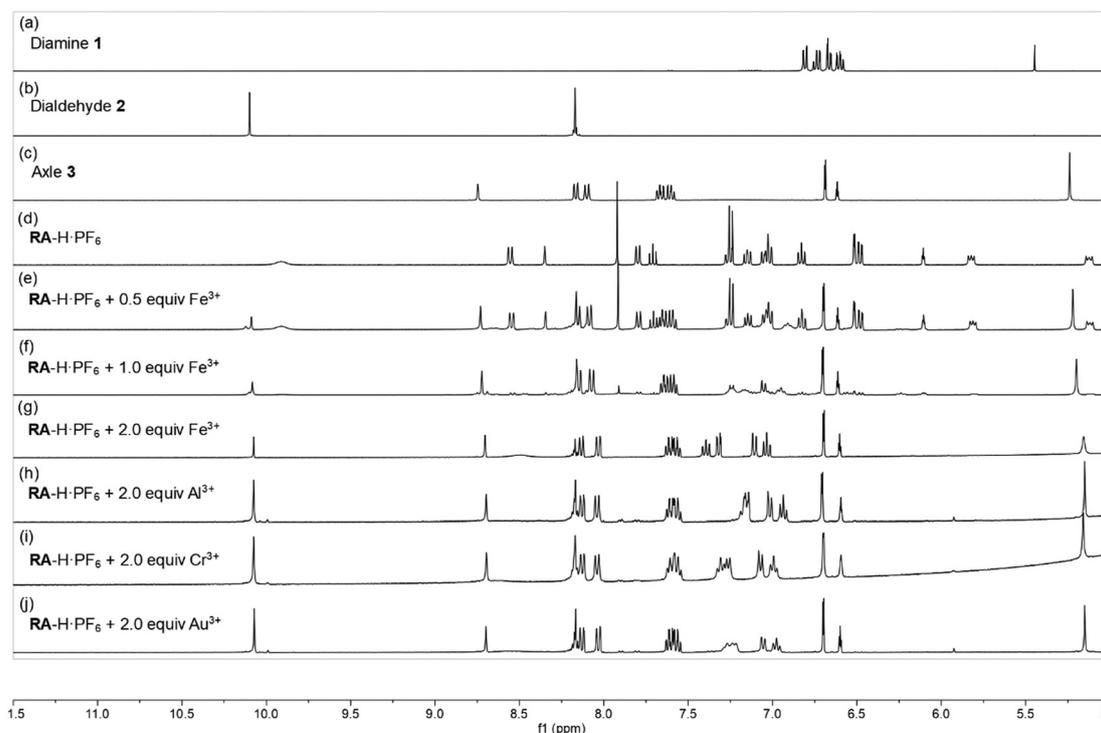


**Fig. 2** Stacked $^1$H NMR spectra (CD$_3$CN, 400 MHz, 298 K) of **RA**-H·PF$_6$ upon the addition of M$^{3+}$ ions: (a) tetraethylene glycol bis(2-aminophenyl)ether, (b) 2,6-pyridine dicarboxaldehyde, (c) anthracene axles **1**, (d) **RA**-H·PF$_6$, (e) **RA**-H·PF$_6$ + 0.5 equiv. of Fe$^{3+}$, (f) **RA**-H·PF$_6$ + 1.0 equiv. of Fe$^{3+}$, (g) **RA**-H·PF$_6$ + 2.0 equiv. of Fe$^{3+}$, (h) **RA**-H·PF$_6$ + 2.0 equiv. of Al$^{3+}$, (i) **RA**-H·PF$_6$ + 2.0 equiv. of Cr$^{3+}$ and (j) **RA**-H·PF$_6$ + 2.0 equiv. of Au$^{3+}$.
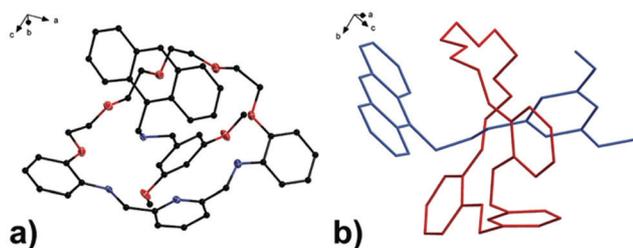
Fig. 3 (a) Perspective view of solid-state structures of reduced [2]rotaxane **RRA**; (b) discriminative view of solid-state structures of reduced [2]rotaxane **RRA**. CCDC code: 1942423.†

MeCN, THF was used to dissolve **RRA**. After the diimine reduction, the fluorescence response of **RRA** in THF/MeCN/$H_2O$ solution (2 : 48 : 50, v/v/v) had more than 50-fold enhancement on fluorescence intensity at 417 nm with 10.0 equiv. of $Au^{3+}$. The fluorescence response has significantly improved and can only be turned on by $Au^{3+}$ (Fig. 4). This suggests that $Au^{3+}$ could inhibit the PET of **RRA**. In comparison with **RRA**, the

response of **RRB** has 1.2-fold enhancement upon the addition of 10.0 equiv. of $Au^{3+}$ and 0.6-fold enhancement upon the addition of 10.0 equiv. of $Hg^{2+}$ and $Cu^{2+}$ separately in MeCN/$H_2O$ solution (50 : 50, v/v). Next, the metal interference on $Au^{3+}$ detection was tested. To study the interference, **RRA** and **RRB** were added to a mixture of $Au^{3+}$ and one of the metal ions used in the previous experiment. The fluorescence response of rotaxanes to $Au^{3+}$ is similar in the presence of most of the metal ions except for $Pd^{2+}$, $Ru^{3+}$ and $V^{3+}$, suggesting that the interference from other metal ions was insignificant (Fig. 4b). The quenching of $Pd^{2+}$, $Ru^{3+}$ and $V^{3+}$ may be due to the similar size with $Au^{3+}$, having an effective ionic radius of 86, 68, 64 and 85 pm respectively.

Since both **RRA** and **RRB** show high selectivity to $Au^{3+}$, NMR titration of $Au^{3+}$ was performed and illustrated (Fig. 5). Upon addition of $Au^{3+}$, the $^1H$ NMR spectra of **RRA** and **RRB** changed dramatically, exhibiting a similar pattern to the acid-equilibrium form of both **RRA** and **RRB**. Moreover, the appearance of ammonium protons ($H_c$) also proved that the dialkylamine of **RRA** ($H_c$ $\delta$ 8.89 ppm) and **RRB** ($H_c$ $\delta$ 8.99 ppm) was protonated by $Au^{3+}$.
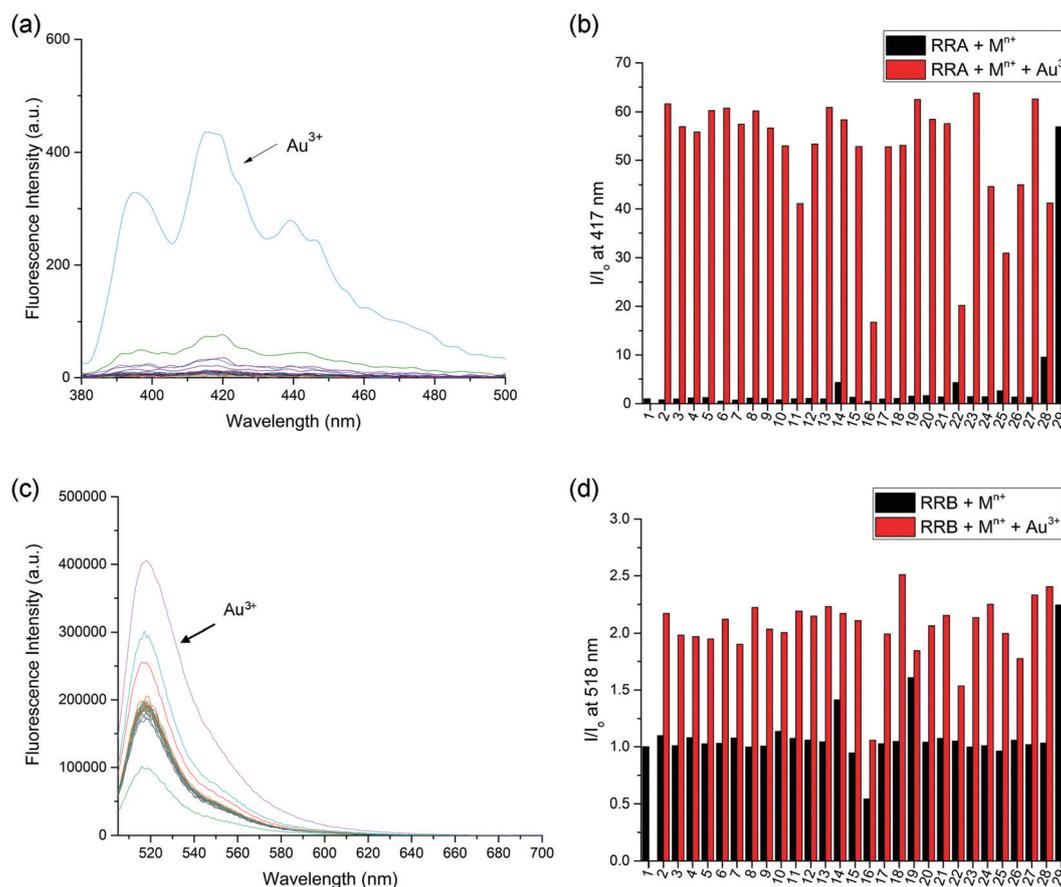


Fig. 4 (a) Fluorescence spectra of **RRA** (20 μM, $\lambda_{ex}$ = 370 nm) with 10 equiv. of $M^{n+}$ in THF/MeCN/$H_2O$ solution (2 : 48 : 50, v/v/v). (b) Fluorescence response of **RRA** (20 μM, $\lambda_{ex}$ = 370 nm) to 10 equiv. of $M^{n+}$ at 417 nm indicated by black bars; **RRA** and different metal ion solutions upon addition of 10 equiv. of $Au^{3+}$ indicated by red bars. (c) Fluorescence spectra of **RRB** (5 μM, $\lambda_{ex}$ = 500 nm) with 10 equiv. of $M^{n+}$ in MeCN/$H_2O$ solution (50 : 50, v/v). (d) Fluorescence response of **RRB** (5 μM, $\lambda_{ex}$ = 500 nm) to 10 equiv. of $M^{n+}$ at 518 nm indicated by black bars; **RRA** and different metal ion solutions upon addition of 10 equiv. of $Au^{3+}$ indicated by red bars. (1) Blank, (2) $Li^+$, (3) $NH_4^+$, (4) $Na^+$, (5) $K^+$, (6) $Ag^+$, (7) $Cs^+$, (8) $Mg^{2+}$, (9) $Ca^{2+}$, (10) $Mn^{2+}$, (11) $Fe^{2+}$, (12) $Co^{2+}$, (13) $Ni^{2+}$, (14) $Cu^{2+}$, (15) $Zn^{2+}$, (16) $Pd^{2+}$, (17) $Cd^{2+}$, (18) $Pt^{2+}$, (19) $Hg^{2+}$, (20) $Pb^{2+}$, (21) $Al^{3+}$, (22) $V^{3+}$, (23) $Cr^{3+}$, (24) $Fe^{3+}$, (25) $Ru^{3+}$, (26) $Rh^{3+}$, (27) $Ce^{3+}$, (28) $Ir^{3+}$ and (29) $Au^{3+}$.

This journal is © The Royal Society of Chemistry and the Chinese Chemical Society 2019

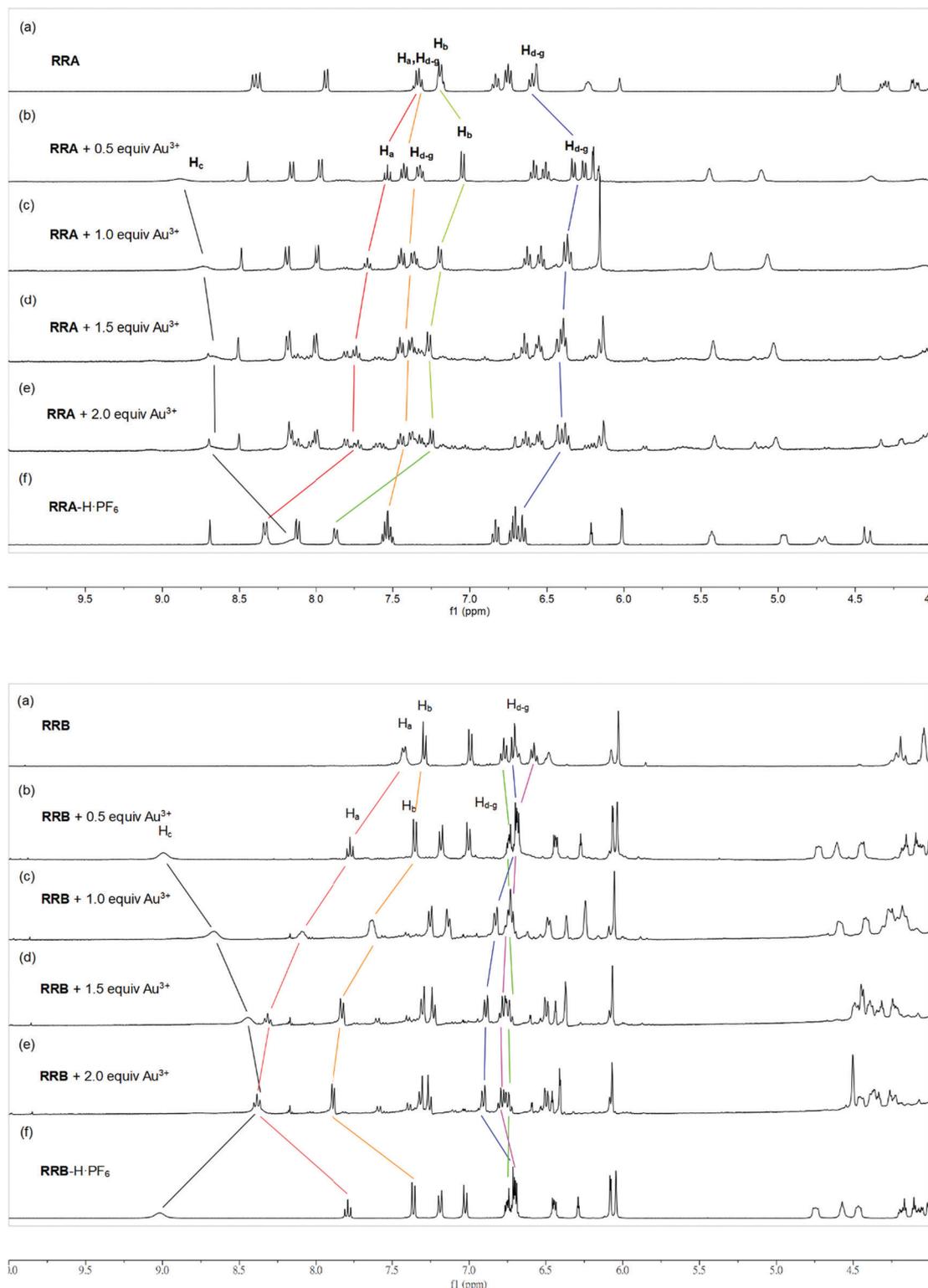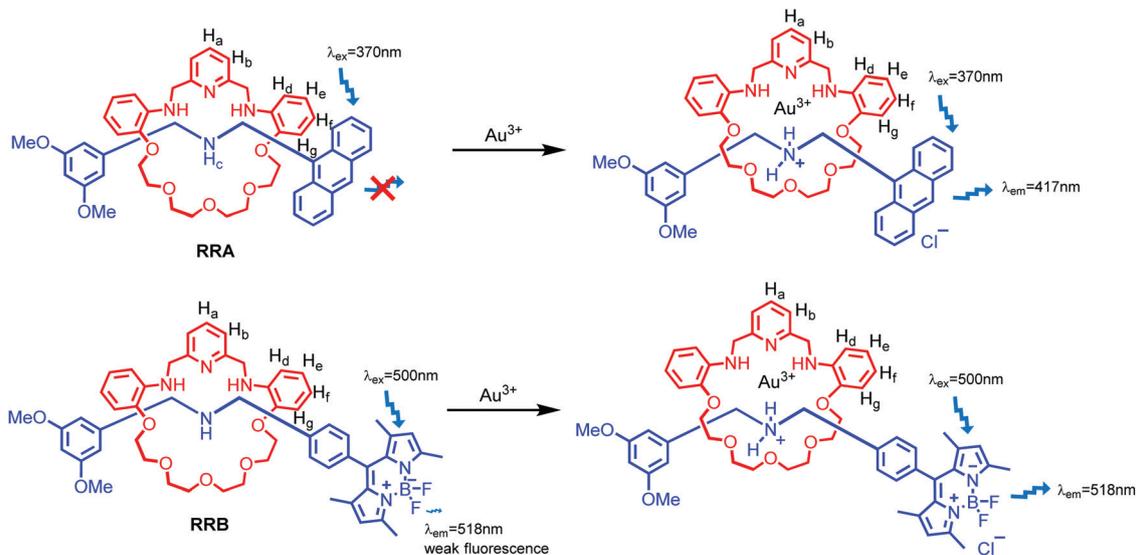*Mater. Chem. Front.*, 2019, **3**, 2388–2396 | **2391**

**Fig. 5** Stacked $^1$H NMR spectra (CD$_3$CN, 400 MHz, 298 K) of **RRA** (upper) and **RRB** (lower) upon addition of (a) 0, (b) 0.5, (c) 1.0 (d) 1.5, and (e) 2.0 equiv. of Au$^{3+}$. (f) **RRA**-H·PF$_6$, and **RRB**-H·PF$_6$.

During the titration, chemical shifts of the pyridyl (H$_{a,b}$), ammonium proton (H$_c$) and phenyl (H$_{d-g}$) units which belong to the macrocyclic ring were observed, indicating their participation in the Au$^{3+}$ complexation. Since the proton signal of both the axle and macrocycle has shifted during the complexation, we proposed that the Au$^{3+}$ was bound inside the cavity of the rotaxanes (Scheme 3).

**2392** | *Mater. Chem. Front.*, 2019, **3**, 2388–2396

This journal is © The Royal Society of Chemistry and the Chinese Chemical Society 2019

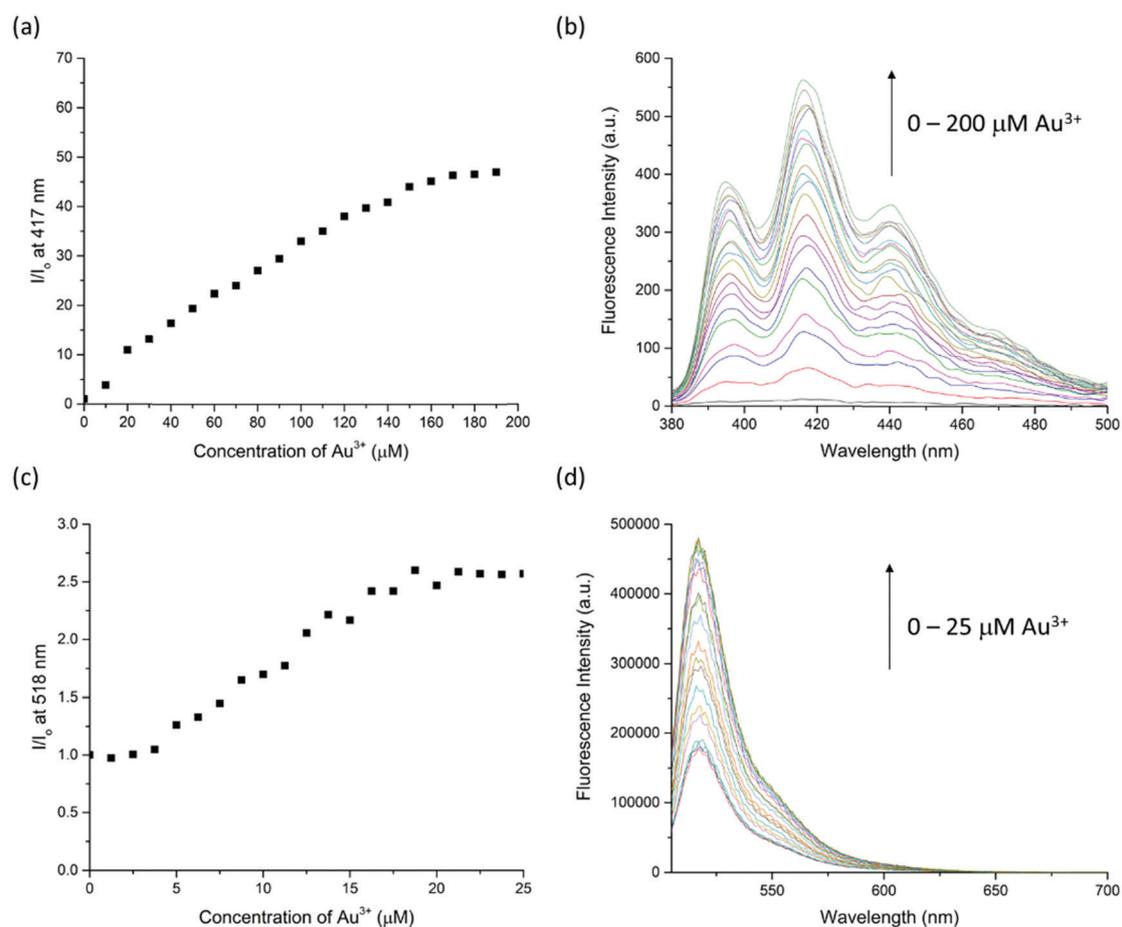**Scheme 3** Plausible mechanism of switch on fluorescence of **RRA** and **RRB** upon addition of $Au^{3+}$.



**Fig. 6** (a) Fluorescence response of **RRA** (20 μM, $\lambda_{ex}$ = 370 nm) at 417 nm upon the addition of $Au^{3+}$ (0–200 μM) in THF/MeCN/$H_2O$ solution (2 : 48 : 50, v/v/v). (b) Fluorescence spectral change of **RRA** (20 μM, $\lambda_{ex}$ = 370 nm) at 417 nm upon addition of $Au^{3+}$ (0–200 μM) in THF/MeCN/$H_2O$ solution (2 : 48 : 50, v/v/v). (c) Fluorescence response of **RRB** (5 μM, $\lambda_{ex}$ = 500 nm) at 518 nm upon the addition of $Au^{3+}$ (0–25 μM) in MeCN/$H_2O$ solution (50 : 50, v/v). (d) Fluorescence spectral change of **RRB** (5 μM, $\lambda_{ex}$ = 500 nm) at 518 nm upon addition of $Au^{3+}$ (0–25 μM) in MeCN/$H_2O$ solution (50 : 50, v/v).
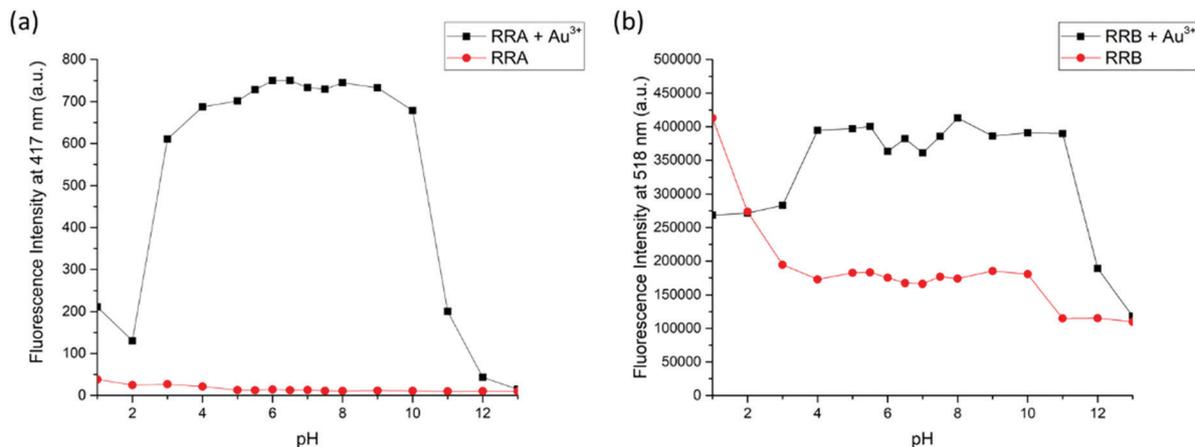
**Fig. 7** (a) Fluorescence response of **RRA** (20 μM, $\lambda_{ex}$ = 370 nm) at 417 nm upon addition of 10 equiv. of $Au^{3+}$ in THF/MeCN/$H_2O$ solution (2 : 48 : 50, v/v/v) (pH 1–13) indicated by the black line; fluorescence of **RRA** at 417 nm in THF/MeCN/$H_2O$ solution (2 : 48 : 50, v/v/v) (pH 1–13) indicated by the red line. (b) Fluorescence response of **RRB** (5 μM, $\lambda_{ex}$ = 500 nm) at 518 nm upon addition of 10 equiv. of $Au^{3+}$ in MeCN/$H_2O$ solution (50 : 50, v/v) (pH 1–13) indicated by the black line; fluorescence of **RRB** at 518 nm in MeCN/$H_2O$ solution (50 : 50, v/v) (pH 1–13) indicated by the red line.

The sensitivity of $Au^{3+}$ detection was studied by a fluorescence titration experiment (Fig. 6). Upon titration, the fluorescence intensity of **RRA** and **RRB** is linearly proportional to the increase of $Au^{3+}$ concentration in the range of 0–160 μM and 5–20 μM, respectively. The intensity remains steady after the addition of 160 μM of $Au^{3+}$ to **RRA** solution and 20 μM of $Au^{3+}$ to **RRB**. The results indicate that the amount of $Au^{3+}$ can be estimated by both rotaxane sensors. Indeed, the binding constant ($K_a$) with **RRA** to $Au^{3+}$ is $9.05 \times 10^3$ $M^{-1}$ and that of

**RRB** with $Au^{3+}$ is $2.92 \times 10^4$ $M^{-1}$, calculated by using the equation $K_a = B^{-1} \times [I_{max} - I_{min}]^{-1}$ from Benesi–Hildebrand analysis (Fig. S2 and S3, ESI†). This reveals that **RRB** can bind stronger to $Au^{3+}$ than **RRA**.

Furthermore, because the NMR titration indicates that **RRA** and **RRB** were acidified during the binding to $Au^{3+}$, the fluorescence response of **RRA** and **RRB** to $Au^{3+}$ can be changed according to the pH equilibrium between the rotaxanes and their protonated form. Therefore, the fluorescence responses of
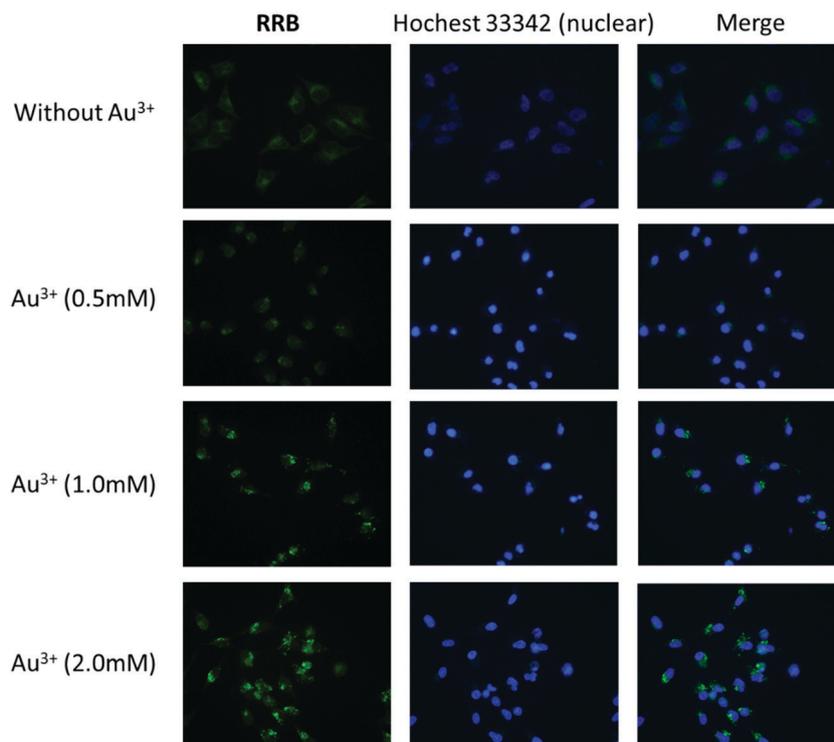


**Fig. 8** Fluorescence images of HeLa cells pretreated with $Au^{3+}$ (0, 0.5, 1.0 and 2.0 mM) for 24 h and then incubated with **RRB** for 2 h. The cell nuclei were stained with Hoechst 33342 (blue) (scale bar: 50 μm).

This journal is © The Royal Society of Chemistry and the Chinese Chemical Society 2019

**RRA** and **RRB** were tested at different pH values (Fig. 7). Without Au$^{3+}$, **RRA** has weak fluorescence in the pH range of 1.0–13.0. While the fluorescence of **RRA** was turned on significantly from pH 4.0–10.0 upon addition of Au$^{3+}$. The results show that the Au$^{3+}$ detection is partially pH independent with **RRA** when the pH is in the range of 4.0–10.0. For **RRB**, it gives weak fluorescence in the pH range of 3.0–13.0 without Au$^{3+}$. Upon addition of Au$^{3+}$, fluorescence was turned on significantly from pH 4.0–11.0. Under extreme acidic conditions, the pyridyl and amine units were protonated, which affects the binding to Au$^{3+}$. Moreover, BODIPY was unstable and could not give reliable sensing results based on fluorescence signals at extremely acidic conditions (pH < 2).[42] Under extreme alkali conditions, the environment facilitates the formation of gold hydroxide, which has a low water solubility ($K_{sp} = 5 \times 10^{-46}$). Without dissolving gold ions in the solution, the formation of a sensor-metal complex is slow, so the fluorescence response of the rotaxanes is greatly reduced.

In addition to the titration experiment, the response time experiment was also conducted to investigate the sensitivity of **RRA** and **RRB** to Au$^{3+}$ (Fig. S4, ESI†). The results show that the fluorescence intensity became steady around 15 min and 5 min for **RRA** and **RRB** respectively, suggesting that both sensors can be used for quick recognition. Moreover, the limit of detection (LOD) of **RRA** for Au$^{3+}$ is 3.23 μM and **RRB** for Au$^{3+}$ is 0.35 μM according to equation: LOD = $3\sigma/m$.

The cell viability of HeLa cells treated with **RRA** and **RRB** for 24 h was assessed using CCK-8 (Fig. S5, ESI†). As a result, the two sensors presented different toxic effects on HeLa cells. For **RRA** treated cells, the viability showed a remarkable decline at 0.2 μM, while the viability in **RRB** treated cells only displayed a slight suppression at 2.0 μM.

Since **RRA** was toxic to the cells even at low concentration (0.2 μM), we only examined the ion detection ability using **RRB** in HeLa cells. It was found that **RRB** could stain the cells and show weak green fluorescence without Au$^{3+}$ treatment (Fig. 8). After the pre-treatment of Au$^{3+}$, the green fluorescence in the cells was obviously enhanced along with the increase of Au$^{3+}$ concentration. Interestingly, the green fluorescence was mostly found in the vacuole-like organelles appearing as green light spots under a fluorescent microscope. This result suggests that **RRB** could detect Au$^{3+}$ and present an ion concentration-dependent sensing capacity in HeLa cells.

## Conclusion

In conclusion, we have synthesized new fluorescent [2]rotaxane sensors. The fluorescence properties of rotaxanes in metal ion detection have been demonstrated. Dynamic rotaxane **RA**-H·PF$_6$ can be hydrolyzed and its fluorescence switched on by common trivalent metal ions. For the reduced form of dynamic rotaxanes, **RRA** and **RRB** have been applied to detect Au$^{3+}$ in 50% H$_2$O in MeCN as a turn-on fluorescent sensor, and the metal interference on Au$^{3+}$ detection is insignificant. Moreover, the fluorescence intensity of rotaxanes is linearly proportional to the concentration of Au$^{3+}$ until excess. **RRB** can be used for Au$^{3+}$ imaging in HeLa cells, demonstrating the application of using mechanically interlocked molecules as imaging probes in biological systems.

## Conflicts of interest

There are no conflicts to declare.

## References

1 R. M. Duke, E. B. Veale, F. M. Pfeffer, P. E. Kruger and T. Gunnlaugsson, *Chem. Soc. Rev.*, 2010, **39**, 3936.
2 X. Zhang, J. Yin and J. Yoon, *Chem. Rev.*, 2014, **114**, 4918.
3 D. Wu, A. C. Sedgwick, T. Gunnlaugsson, E. U. Akkaya, J. Yoon and T. D. James, *Chem. Soc. Rev.*, 2017, **46**, 7105.
4 N. De Acha, C. Elosúa, M. J. Corres and J. F. Arregui, *Sensors*, 2019, 19.
5 J. F. Stoddart and H. M. Colquhoun, *Tetrahedron*, 2008, **64**, 8231.
6 C. J. Bruns and J. F. Stoddart, *The Nature of the Mechanical Bond*, John Wiley & Sons, Inc., Hoboken, NJ, USA, 2016.
7 M. J. Langton and P. D. Beer, *Acc. Chem. Res.*, 2014, **47**, 1935.
8 M. Cirulli, A. Kaur, J. E. M. Lewis, Z. Zhang, J. A. Kitchen, S. M. Goldup and M. M. Roessler, *J. Am. Chem. Soc.*, 2019, **141**, 879.
9 K. Hiratani, M. Kaneyama, Y. Nagawa, E. Koyama and M. Kanesato, *J. Am. Chem. Soc.*, 2004, **126**, 13568.
10 M. Denis, J. Pancholi, K. Jobe, M. Watkinson and S. M. Goldup, *Angew. Chem., Int. Ed.*, 2018, **57**, 5310.
11 L. M. Hancock, L. C. Gilday, S. Carvalho, P. J. Costa, V. Félix, C. J. Serpell, N. L. Kilah and P. D. Beer, *Chem. – Eur. J.*, 2010, **16**, 13082.
12 T. Shukla, A. K. Dwivedi, R. Arumugaperumal, C. M. Lin, S. Y. Chen and H. C. Lin, *Dyes Pigm.*, 2016, **131**, 49.
13 X. Wang, J. Zhu and D. B. Smithrud, *J. Org. Chem.*, 2010, **75**, 3358.
14 S.-Y. Hsueh, C.-C. Lai and S.-H. Chiu, *Chem. – Eur. J.*, 2010, **16**, 2997.
15 W. Zhou, J. Li, X. He, C. Li, J. Lv, Y. Li, S. Wang, H. Liu and D. Zhu, *Chem. – Eur. J.*, 2008, **14**, 754.
16 R. Arumugaperumal, V. Srinivasadesikan, M. V. Ramakrishnam Raju, M.-C. Lin, T. Shukla, R. Singh and H.-C. Lin, *ACS Appl. Mater. Interfaces*, 2015, **7**, 26491.

This journal is © The Royal Society of Chemistry and the Chinese Chemical Society 2019

*Mater. Chem. Front.*, 2019, **3**, 2388–2396 | **2395**

17 J. Y. C. Lim, I. Marques, V. Félix and P. D. Beer, *J. Am. Chem. Soc.*, 2017, **139**, 12228.

18 J. Y. C. Lim, I. Marques, V. Félix and P. D. Beer, *Angew. Chem., Int. Ed.*, 2018, **57**, 584.

19 Y.-C. Yeh, B. Creran and V. M. Rotello, *Nanoscale*, 2012, **4**, 1871.

20 C. F. Shaw, *Chem. Rev.*, 1999, **99**, 2589.

21 I. Ott, *Coord. Chem. Rev.*, 2009, **253**, 1670.

22 A. S. K. Hashmi, *Chem. Rev.*, 2007, **107**, 3180.

23 D. Pflästerer and A. S. K. Hashmi, *Chem. Soc. Rev.*, 2016, **45**, 1331.

24 R. Ciriminna, E. Falletta, C. Della Pina, J. H. Teles and M. Pagliaro, *Angew. Chem., Int. Ed.*, 2016, **55**, 14210–14217.

25 A. Habib and M. Tabata, *J. Inorg. Biochem.*, 2004, **98**, 1696.

26 A. Kundu, R. K. Layek, A. Kuila and A. K. Nandi, *ACS Appl. Mater. Interfaces*, 2012, **4**, 5576.

27 E. E. Connor, J. Mwamuka, A. Gole, C. J. Murphy and M. D. Wyatt, *Small*, 2005, **1**, 325.

28 P. T. Glink, A. I. Oliva, J. F. Stoddart, A. J. P. White and D. J. Williams, *Angew. Chem., Int. Ed.*, 2001, **40**, 1870.

29 M. Horn, J. Ihringer, P. T. Glink and J. F. Stoddart, *Chem. – Eur. J.*, 2003, **9**, 4046.

30 J. Wu, K. C.-F. Leung and J. F. Stoddart, *Proc. Natl. Acad. Sci. U. S. A.*, 2007, **104**, 17266.

31 M. E. Belowich, C. Valente and J. F. Stoddart, *Angew. Chem., Int. Ed.*, 2010, **49**, 7208.

32 A.-J. Avestro, D. M. Gardner, N. A. Vermeulen, E. A. Wilson, S. T. Schneebeli, A. C. Whalley, M. E. Belowich, R. Carmieli, M. R. Wasielewski and J. F. Stoddart, *Angew. Chem., Int. Ed.*, 2014, **53**, 4442.

33 Z. Li, X. Han, H. Chen, D. Wu, F. Hu, S. H. Liu and J. Yin, *Org. Biomol. Chem.*, 2015, **13**, 7313.

34 X. Han, Z. Li, Z. Xu, Z. Zhao, S. H. Liu and J. Yin, *Chin. J. Chem.*, 2017, **35**, 1050.

35 Z. Li, C. He, Y. Li, Y. Wang, C. Wei, J. Yin and S. H. Liu, *Dyes Pigm.*, 2018, **148**, 130.

36 Y.-H. Chang, Y.-J. Lee, C.-C. Lai, Y.-H. Liu, S.-M. Peng and S.-H. Chiu, *Org. Lett.*, 2018, **20**, 2416.

37 V. Dvornikovs, B. E. House, M. Kaetzel, J. R. Dedman and D. B. Smithrud, *J. Am. Chem. Soc.*, 2003, **125**, 8290.

38 A. Fernandes, A. Viterisi, F. Coutrot, S. Potok, D. A. Leigh, V. Aucagne and S. Papot, *Angew. Chem., Int. Ed.*, 2009, **48**, 6443.

39 R. Barat, T. Legigan, I. Tranoy-Opalinski, B. Renoux, E. Péraudeau, J. Clarhaut, P. Poinot, A. E. Fernandes, V. Aucagne, D. A. Leigh and S. Papot, *Chem. Sci.*, 2015, **6**, 2608.

40 G. Yu, D. Wu, Y. Li, Z. Zhang, L. Shao, J. Zhou, Q. Hu, G. Tang and F. Huang, *Chem. Sci.*, 2016, **7**, 3017.

41 W.-Y. Wong, K. C.-F. Leung and J. F. Stoddart, *Org. Biomol. Chem.*, 2010, **8**, 2332.

42 M. Baruah, W. Qin, C. Flors, J. Hofkens, R. A. L. Vallée, D. Beljonne, M. Van der Auweraer, W. M. De Borggraeve and N. Boens, *J. Phys. Chem. A*, 2006, **110**, 5998.